

Self-Supervised Learning for 3D Medical Image Analysis using 3D SimCLR and Monte Carlo Dropout

Yamen Ali

TU Berlin, Germany

YAMEN.ALI@TU-BERLIN.DE

Aiham Taleb

HPI, Germany

AIHAM.TALEB@HPI.DE

Marina M.-C. Höhne

TU Berlin, Germany

MARINA.HOEHNE@TU-BERLIN.DE

Christoph Lippert

HPI, Germany

CHRISTOPH.LIPPERT@HPI.DE

Abstract

Self-supervised learning methods can be used to learn meaningful representations from unlabeled data that can be transferred to supervised downstream tasks to reduce the need for labeled data. In this paper, we propose a 3D self-supervised method that is based on the contrastive (SimCLR) method. Additionally, we show that employing Bayesian neural networks (with Monte-Carlo Dropout) during the inference phase can further enhance the results on the downstream tasks. We showcase our models on two medical imaging segmentation tasks: i) Brain Tumor Segmentation from 3D MRI, ii) Pancreas Tumor Segmentation from 3D CT. Our experimental results demonstrate the benefits of our proposed methods in both downstream data-efficiency and performance.

Keywords: Self-supervised learning, Image segmentation, SimCLR, Monte-Carlo Dropout

1. Introduction

As 3D medical imaging became an essential tool in medicine, the need for accurate and reliable machine learning algorithms that analyze such images has become more apparent. However, acquiring sufficient amounts of annotated 3D images is a non-trivial task due to the challenges related to privacy issues or the sheer time and cost required to get expert annotations for such data. Hence, this motivates other solutions to address the scarcity of annotations.

Self-Supervised Learning (SSL) has proven to be a powerful technique that allows constructing meaningful representations for the images by applying

pretext tasks on the unlabelled data, e.g. [Taleb et al. \(2020\)](#); [Tajbakhsh et al. \(2020\)](#); [Zhou et al. \(2019\)](#). [Chen et al. \(2020\)](#) introduced a novel *Simple* framework for *Contrastive Learning* of visual *Representations* (SimCLR). SimCLR leverages the normalized temperature-scaled cross-entropy loss (NT-Xent) in order to maximize the similarity between latent space representations of various augmentations of the same data point. In their work, they show how the representations learned from SimCLR can achieve state-of-the-art results when used in the downstream tasks of 2D natural image classification.

Our contributions: We introduce a method to utilize SimCLR in volumetric 3D image segmentation. Our method addresses the inherent challenges in semantic segmentation on 3D scans such as imbalanced classes and the expensive process of data annotation. Moreover, we show that the additional inclusion of uncertainties through approximate Bayesian weight inference in the form of Monte Carlo (MC) Dropout in the self-supervised algorithm significantly enhances the performance on segmentation tasks.

2. Method

Our approach consists of three main steps. We start by a self-supervised learning step that results in a trained encoder g_{enc} . In the second step, we fine-tune the encoder g_{enc} with the downstream task, e.g. segmentation task, using the annotated data. Finally, in the third step, we apply MC Dropout during prediction and report the dice scores on the test data.

2.1. Pretask Training

In the following, we propose a pretask that generalizes SimCLR to volumetric 3D inputs such that the full 3D spatial context of the scans is explored. We start by randomly sampling a batch of M 3D scans, then each 3D scan is split into P equally-sized non-overlapping 3D patches resulting in $N = M * P$ input samples. Before processing the input by the model, two random composite augmentations (chosen from: 3D rotation with different angles on one or more axis, color distortion, identity, Gaussian noise, Gaussian blur, and Sobel filtering) are applied onto each 3D patch leading to a dataset size of $2N$. Hence, similar as in SimCLR there exists one positive pair for every input sample, i.e., one pair originating from the same original 3D patch, and $2(N - 1)$ negative pairs, i.e., originating from different 3D patches.

2.1.1. MODEL ARCHITECTURE & LOSS

The model architecture used for the pretask is similar to the one proposed in [Chen et al. \(2020\)](#), consisting of an encoder g_{enc} (3D-CNN) followed by a non-linear projection head (Dense layer). As loss function we used a normalized temperature-scaled cross entropy to compute the loss for a positive pair of two augmented 3D patches z_i and z_j in the latent space representations (i.e. dense layer output):

$$l_{i,j} = -\log \frac{\exp(sim(z_i, z_j)/\tau)}{\sum_{k=1}^{2N} 1_{[k \neq i]} \exp(sim(z_i, z_k)/\tau)} \quad (1)$$

where sim is the cosine similarity and τ the temperature parameter.

2.2. Finetuning

To perform the required downstream segmentation task we keep only the pretrained encoder g_{enc} without the non-linear projection head. The encoder outputs are passed to a decoder g_{dec} and the model, a U-Net proposed by [Ronneberger et al. \(2015\)](#), is trained in a supervised manner using the annotated 3D scans. As a loss function, the weighted dice score is used in order to maximize the intersection-over-union ratio between the model predictions and the ground truth across all classes. Formally expressed as:

$$Dice = -\frac{1}{N} \sum_{i=1}^N \frac{2(\sum_{j=1}^M Y_{ij} \times T_{ij}) + s}{(\sum_{j=1}^M Y_{ij} + \sum_{j=1}^M T_{ij}) + s} \quad (2)$$

where Y_{ij} is the probability that pixel j belongs to class i , T_{ij} is the ground truth indicator, which is 1

if pixel j belongs to class i and 0 otherwise, s is a smoothing parameter (otherwise called epsilon), N is the number of classes, and M is the number of pixels.

2.3. Bayesian Approximation

Usually the predicted segmentation mask is deterministic and we lack information about the models certainty of the pixel-wise predictions. However, as shown in [Gal and Ghahramani \(2016\)](#), MC dropout can be used as a Bayesian approximation method. Accordingly, we obtain uncertainty estimates on the predicted segmentation, by applying MC dropout during the testing phase. Descriptively, this can be seen as a procedure, where, instead of sampling from a learned posterior distribution on the weights, we apply dropout during testing, thus obtaining a subset of weights that define a sampled sub-network. Note that the number of networks we sample via dropout is a hyperparameter, that needs to be set. The predictions of the individual sub-networks follow the multimodality strategies learned in the network and can be aggregated in various ways to achieve more transparency regarding the models certainty. We investigate the following four different aggregation methods:

- **Majority:** A pixel labeled with the class, where the majority of the networks agreed on.
- **Weighted Majority:** Additionally to the Majority aggregation, each class is multiplied by a weight to enable a class specific prioritizing.
- **Borda:** For each pixel-wise prediction, points are distributed, such that the class with the highest probability has the most points and the class with the lowest probability the fewest points. Then the points of all sub-networks are added pixel-wise and class label that has achieved the most points is assigned to the pixel.
- **Union per $class_x$:** Given a class of interest, a pixel is assigned to that class if at least one sub-network predicts this class for that pixel. This prediction aggregation encourages the algorithm to be sensitive to specific classes, e.g. Tumor. However, such approach affects the overall dice score as it produces more false positives.

3. Experimental Results & Conclusion

In this section, we show some initial results of applying our 3D SimCLR approach to two datasets:

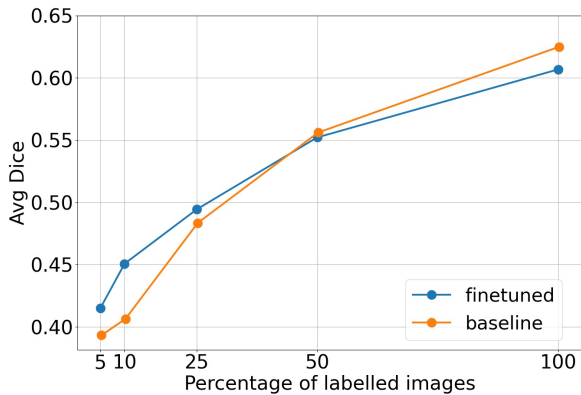


Figure 1: Visualization of the average dice score (y-axis) for the pancreas test dataset when finetuning the model with 5%, 10%, 25%, 50%, 100% of the training dataset (x-axis). Our proposed 3D SimCLR approach (blue line) outperforms the baseline approach (orange line) when less than 25% of labeled data are available.

the Pancreas tumor segmentation dataset by Simpson et al. (2019) and the Brain tumor segmentation dataset by Menze et al. (2015). Then, we evaluate the impact of MC dropout on the model performance.

3.1. Pancreas Dataset Results

This dataset from the medical Decathlon benchmark Simpson et al. (2019) contains 3D CT scans of Pancreas tumors. It consists of 420 scans with only 281 of them being annotated. Each scan consists of voxels from 3 classes: background, pancreas, and tumor. All 420 scans are used during the pretask training phase. For the fine-tuning, we split the 281 annotated scans into a training set of 197 scans, and a test set of 84 scans, which is only used for evaluation. Figure 1 shows the improvement obtained by using the pretask encoder during finetuning, when only up to 25% of the labeled data is available. The Pancreas dataset is challenging in nature due to the fact that the Pancreas and tumor classes occupy only a small area of the scan, i.e. a class imbalance.

3.2. Brain Dataset Results

The multimodal Brain Tumor Segmentation 2018 benchmark Menze et al. (2015) dataset consists of 351 scans, out of which 285 are annotated. Each scan contains voxels from 4 classes: background, whole tumor, tumor core, and enhanced tumor. All 351 scans are used during the pretask training phase. For the fine

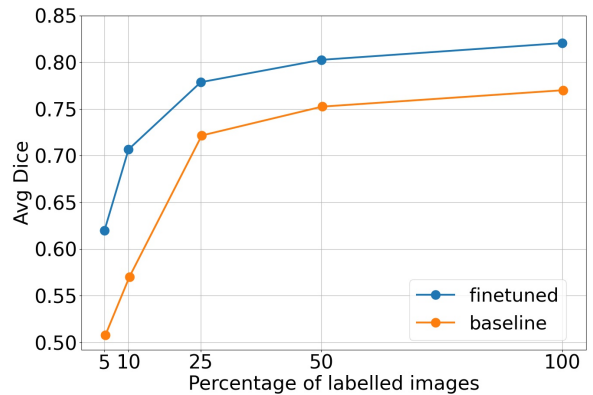


Figure 2: Average dice score of the Brats test dataset predictions when the model is fine-tuned using 5%, 10%, 25%, 50%, 100% of the training dataset

tuning, we split the 285 annotated scans into a training set of 200 scans and a test set of 85 scans, which is only used for evaluation. The improvement obtained by using the pretask encoder in finetuning, as shown in Figure 2, is more nuanced than in the Pancreas dataset. This can be attributed to the scans' nature where the tumor covers a larger area which reduces the effects of class imbalance.

3.3. Monte-Carlo Dropout Results

Figure 3 shows that applying MC dropout improves the accuracy of the fine-tuned model, while the baseline model accuracy hardly changes. We conjecture this to be because the weights of the fine-tuned encoder, sampled by MC dropout, contain more useful features than their counterparts in the baseline's encoder. To verify the previous hypothesis, we run the MC dropout algorithm on the fine-tuned model with dropout enabled only on the encoder, only on the decoder, and on both of them. As Figure 4 shows, the major improvement of the dice score occurs only when dropout is performed on the encoder. The decoder alone is not sufficient to obtain such an improvement. Figure 5 shows how different dropout rates affect the improvement due to the MC Dropout algorithm. It also shows that a higher dropout rate, e.g. 0.5, adversely affects the results as it would introduce more noise during the inference.

In Figure 6, we compare the different prediction aggregations presented in Section 2.3 on the Pancreas dataset with encoder dropout rate 0.3 and decoder dropout 0.0. We can observe that these aggregation

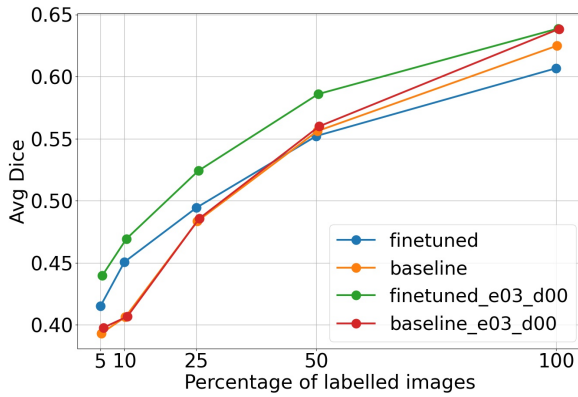


Figure 3: Comparison between the Pancreas fine-tuned and baseline models average dice scores before and after applying MC Dropout with 100 Iterations, encoder dropout=0.3, decoder dropout=0.0, and the majority voting protocol

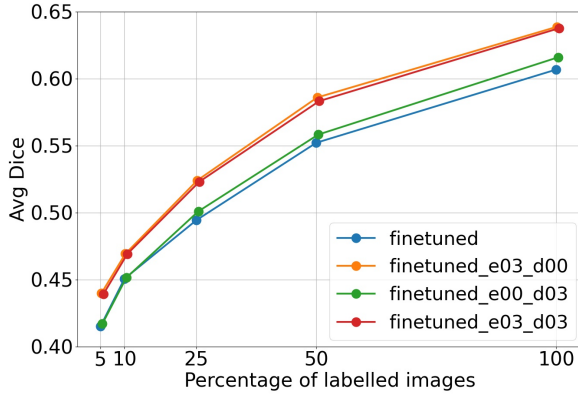


Figure 4: Comparison of MC dropout configurations in terms of average dice score when fine-tuning on Pancreas

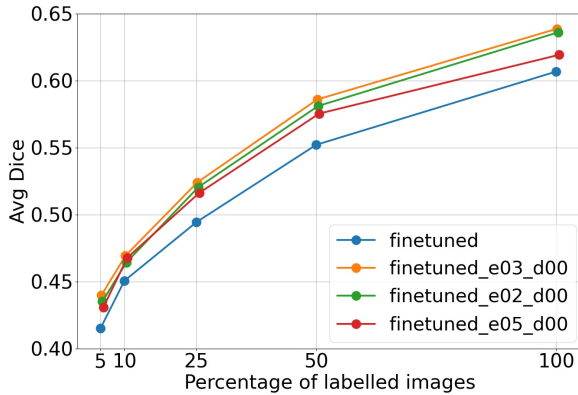


Figure 5: Comparison of different dropout rates in terms of average dice score when fine-tuning models on Pancreas

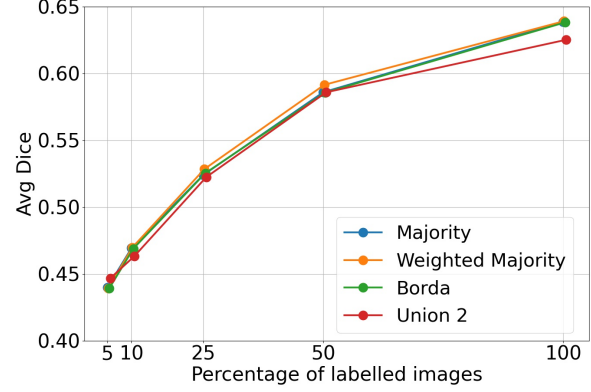


Figure 6: Comparison of the different prediction aggregation methods presented in Section 2.3.

methods have a similar performance, whereby the Weighted Majority ($background = 1$, $Pancreas = 2$, $tumor = 2$) performs slightly better when over 5% of labeled data are available. The Borda and Majority protocols give almost identical results, indicating that the network predictions strongly agree.

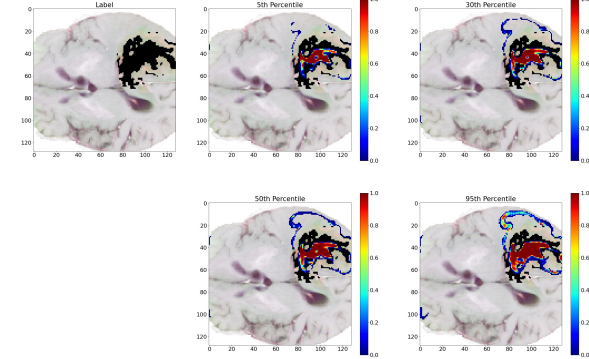


Figure 7: Heat-maps of different percentiles of the WT class predictions for a sample from the BraTS dataset. The black pixels represent the true WT.

Finally, in order to visualize the uncertainty knowledge gained by using MC dropout as a Bayesian approximation method, we compute pixel-wise different percentiles of the predictions and plot them as a heatmap over the Whole Tumor(WT) segmentation (black area) as shown in Figure 7 for the BraTS scan, with 100 MC Dropout steps (100 networks) similar as in [Bykov et al. \(2021\)](#). Those heatmaps can be interpreted as a confidence indication that MC dropout networks have on pixel assignments, where the 5th percentile heatmap indicates the most certain area

for WT (red=certain, blue=uncertain) as being in the middle of the WT area. From the 95th percentile heat map, we can observe a higher overlap with the true WT segmentation, however, the false positive rate increased as expected.

In conclusion, our experimental results demonstrate the potential of our proposed 3D SimCLR method, nested with additional models uncertainty information gained by Bayesian approximation at inference time, in terms of downstream data efficiency and performance improvement. These findings encourage further research in this direction, especially for annotation-starved healthcare applications.

References

Kirill Bykov, Marina M.-C. Höhne, Adelaida Creosteanu, Klaus-Robert Müller, Frederick Klauschen, Shinichi Nakajima, and Marius Kloft. Explaining bayesian neural networks. *CoRR*, abs/2108.10346, 2021. URL <https://arxiv.org/abs/2108.10346>.

Ting Chen, Simon Kornblith, Mohammad Norouzi, and Geoffrey Hinton. A simple framework for contrastive learning of visual representations. In Hal Daumé III and Aarti Singh, editors, *Proceedings of the 37th International Conference on Machine Learning*, volume 119 of *Proceedings of Machine Learning Research*, pages 1597–1607. PMLR, 13–18 Jul 2020. URL <https://proceedings.mlr.press/v119/chen20j.html>.

Yarin Gal and Zoubin Ghahramani. Dropout as a bayesian approximation: Representing model uncertainty in deep learning. In Maria Florina Balcan and Kilian Q. Weinberger, editors, *Proceedings of The 33rd International Conference on Machine Learning*, volume 48 of *Proceedings of Machine Learning Research*, pages 1050–1059, New York, New York, USA, 20–22 Jun 2016. PMLR. URL <https://proceedings.mlr.press/v48/gal16.html>.

Bjoern H. Menze, Andras Jakab, Stefan Bauer, Jayashree Kalpathy-Cramer, Keyvan Farahani, Justin Kirby, Yuliya Burren, and et al. The multi-modal brain tumor image segmentation benchmark (brats). *IEEE Transactions on Medical Imaging*, 34(10):1993–2024, 2015. URL <https://ieeexplore.ieee.org/document/6975210>.

Olaf Ronneberger, Philipp Fischer, and Thomas Brox. U-net: Convolutional networks for biomedical image segmentation. In *Medical Image Computing and Computer-Assisted Intervention (MICCAI)*, volume 9351 of *LNCS*, pages 234–241. Springer, 2015. URL <http://lmb.informatik.uni-freiburg.de/Publications/2015/RFB15a>.

Amber L. Simpson, Michela Antonelli, Spyridon Bakas, Michel Bilello, Keyvan Farahani, Bram van Ginneken, Annette Kopp-Schneider, Bennett A. Landman, and et al. A large annotated medical image dataset for the development and evaluation of segmentation algorithms. *CoRR*, abs/1902.09063, 2019. URL <http://arxiv.org/abs/1902.09063>.

Nima Tajbakhsh, Laura Jeyaseelan, Qian Li, Jeffrey N. Chiang, Zhihao Wu, and Xiaowei Ding. Embracing imperfect datasets: A review of deep learning solutions for medical image segmentation. *Medical Image Analysis*, 63:101693, 2020. ISSN 1361-8415. doi: <https://doi.org/10.1016/j.media.2020.101693>. URL <http://www.sciencedirect.com/science/article/pii/S136184152030058X>.

Aiham Taleb, Winfried Loetzsch, Noel Danz, Julius Severin, Thomas Gaertner, Benjamin Bergner, and Christoph Lippert. 3d self-supervised methods for medical imaging. In H. Larochelle, M. Ranzato, R. Hadsell, M. F. Balcan, and H. Lin, editors, *Advances in Neural Information Processing Systems*, volume 33, pages 18158–18172. Curran Associates, Inc., 2020. URL <https://proceedings.neurips.cc/paper/2020/file/d2dc6368837861b42020ee72b0896182-Paper.pdf>.

Zongwei Zhou, Vatsal Sodha, Md Mahfuzur Rahman Siddiquee, Ruibin Feng, Nima Tajbakhsh, Michael B. Gotway, and Jianming Liang. Models genesis: Generic autodidactic models for 3d medical image analysis. In *Medical Image Computing and Computer Assisted Intervention – MICCAI 2019*, pages 384–393, Cham, 2019. Springer International Publishing. ISBN 978-3-030-32251-9. URL https://link.springer.com/chapter/10.1007/978-3-030-32251-9_42.

Appendix A. Datasets Samples

Figure 8(a) and Figure 8(b) show a slice in Pancreas and BraTS 3D scans. We notice how the Pancreas tumor region is smaller than the Brain tumor region which makes the segmentation task on the Pancreas dataset intrinsically more challenging.

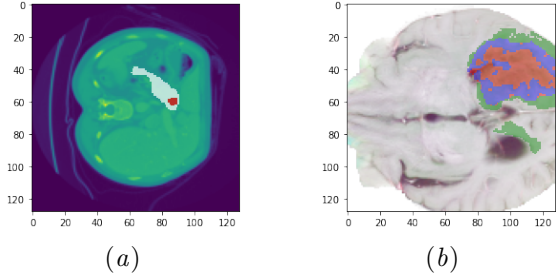


Figure 8: (a) A 2D slice from a Pancreas scan. The white area is the Pancreas, red is the tumor, and the rest is background. (b) A 2D slice from a BraTS scan. The green area is the whole tumor, red is the tumor core, blue is the enhanced tumor, and the rest is background

Appendix B. Training Details

B.1. Data preprocessing

As a preprocessing step on both datasets, a bounding box which surrounds the organs along each axis is found and all voxels outside this box are cropped out in order to reduce the amount of background voxels. Furthermore, all scans are resized into a unified resolution of $128 \times 128 \times 128$.

B.2. Pretask Training

For the temperature value in the Equation (1) we experimented with the same values suggested by [Chen et al. \(2020\)](#), namely (0.05, 0.1, 0.5). For all the previously mentioned self supervised trained encoders, the temperature was set to (0.05) and the training ran for 1000 epochs.

B.3. Fine-tuning

Both the fine-tuned model and the baseline model were trained for 400 epochs. But for the fine-tuned model, we follow a warm-up procedure suggested by [Taleb et al. \(2020\)](#) where we freeze the encoder weights for the first 25 epochs. The smoothing value in Equation (2) is set to 1×10^{-5} .